THE JOURNAL OF PHYSICAL CHEMISTRY C

Article

pubs.acs.org/JPCC

New Functionalized Metal−Organic Frameworks MIL-47-X (X = −Cl, −Br, $-CH_3$, $-CF_3$, −OH, $-OCH_3$): Synthesis, Characterization, and CO_2 Adsorption Properties

Shyam Biswas,[†] Danny E. P. Vanpoucke,[‡] Toon Verstraelen,[‡] Matthias Vandichel,[‡] Sarah Couck,[§] Karen Leus,[†] Ying-Ya Liu,[†] Michel Waroquier,[‡] Veronique Van Speybroeck,[‡] Joeri F. M. Denayer,[§] and Pascal Van Der Voort*[,†]

[†]Department of Inorganic and Physical Chemistry, Centre for Ordered Materials, Organometallics and Catalysis, Ghent University, Krijgslaan 281-S3, 9000 Ghent, Belgium

[‡]Center for Molecular Modeling, Universiteit Gent, Technologiepark 903, 9052 Zwijnaarde, Belgium

[§]Department of Chemical Engineering, Vrije Universiteit Brussel, Pleinlaan 2, 1050 Brussel, Belgium

Supporting Information

ABSTRACT: Six new functionalized vanadium hydroxo terephthalates [V^{III}(OH)(BDC-X)]·n(guests) (MIL-47(V^{III})-X-AS) (BDC = 1,4-benzenedicarboxylate; X = −Cl, −Br, $-CH_3$, $-CF_3$, −OH, $-OCH_3$; AS = as-synthesized) along with the parent MIL-47 were synthesized under rapid microwave-assisted hydrothermal conditions (170 °C, 30 min, 150 W). The unreacted H_2BDC-X and/or occluded solvent molecules can be removed by thermal activation under vacuum, leading to the empty-pore forms of the title compounds (MIL-47(V^{IV})-X). Except pristine MIL-47 (+III oxidation state), the vanadium atoms in all the evacuated functionalized solids stayed in the +IV oxidation state. The phase purity of the compounds was ascertained by X-ray powder diffraction (XRPD), diffuse reflectance infrared Fourier transform (DRIFT) spectroscopy, Raman, thermogravimetric (TG), and elemental analysis. The structural similarity of the filled and empty-pore forms of the functionalized compounds with the respective forms of parent MIL-47 was verified by cell parameter determination from XRPD data. TGA and temperature-dependent XRPD (TDXRPD) experiments in an air atmosphere indicate high thermal stability in the 330−385 °C range. All the thermally activated compounds exhibit significant microporosity (S_{BET} in the 305−897 $m^2\ g^{-1}$ range), as verified by the N_2 and CO_2 sorption analysis. Among the six functionalized compounds, MIL-47(V^{IV})-OCH_3 shows the highest CO_2 uptake, demonstrating the determining role of functional groups on the CO_2 sorption behavior. For this compound and pristine MIL-47(V^{IV}), Widom particle insertion simulations were performed based on ab initio calculated crystal structures. The theoretical Henry coefficients show a good agreement with the experimental values, and calculated isosurfaces for the local excess chemical potential indicate the enhanced CO_2 affinity is due to two effects: (i) the interaction between the methoxy group and CO_2 and (ii) the collapse of the MIL-47(V^{IV})-OCH_3 framework.

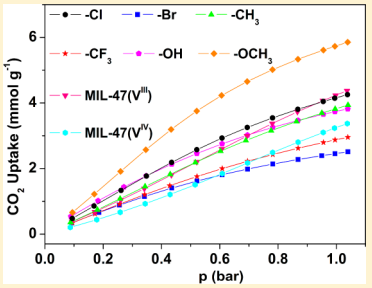

1. INTRODUCTION

Metal−organic frameworks (MOFs),[1] which are a class of highly crystalline and porous materials, have attracted considerable interest in recent years because of their possible applications in a broad range of areas such as gas storage and separation,[2] catalysis,[3] and drug delivery.[4] They are constructed from inorganic building units and polytopic organic linkers. The pore characteristics (dimensions or chemical nature) of a particular MOF can be tuned in a systematic fashion without altering the underlying topology by introducing functional groups (having different dimensions, polarities, acidities, etc.) to the organic linker. The introduction of such functionalities to the organic moiety can be achieved (i) by directly using prefunctionalized linkers during synthesis or (ii) by a postsynthetic modification approach.[5] Both strategies have been successfully employed for functionalization of rigid as well as flexible (often termed "breathing") MOFs. The functionalization of rigid MOFs affects their sorption[6,7] and selectivity[8] as well as thermal and chemical stability.[9] In addition to tuning these properties, the functionalization of flexible MOFs can influence their breathing characteristics (i.e., magnitude of pore opening and closing).[10,11]

Among the various topological framework types known for MOFs, the MIL-n family of materials originally developed by Férey's group and a few others are of the greatest interest because of their high thermal and hydrolytic stability as well as intrinsic porosity.[12,13] For example, the thermally activated form of the vanadium-based terephthalate MIL-47 with the formula [V^{IV}(O)(BDC)] (BDC = 1,4-benzenedicarboxylate) possesses a large BET surface area of 930 $m^2\ g^{-1}$ and a high

Received: July 11, 2013
Revised: October 16, 2013
Published: October 17, 2013

   dx.doi.org/10.1021/jp406835n | J. Phys. Chem. C 2013, 117, 22784−22796

thermal stability of 400 °C in air.[14] The structure of MIL-47 (Figure 1) contains chains of *trans* corner-sharing [$V^{IV}O_6$]

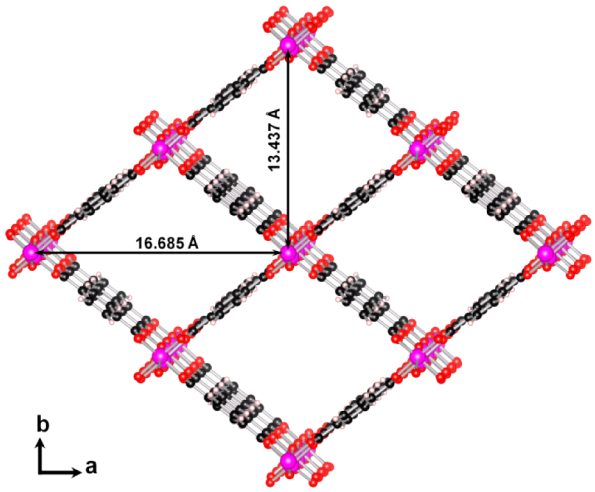

Figure 1. Ball-and-stick model of the MIL-47(V^{IV}) structure. V atomic positions are indicated by the big pink spheres surrounded by an octahedron of O atoms (small red spheres). Black and white spheres indicate the C and H atomic positions, respectively, of the organic linker. Lattice parameters, as calculated for the fully relaxed structure (cf. Table 3), are indicated.

octahedra that are connected with each other by BDC linkers to form a three-dimensional framework having a one-dimensional pore system. The thermal activation of MIL-47(V^{III})-AS in an air atmosphere results in MIL-47(V^{IV}), which shows a rigid large pore (LP) structure due to the absence of μ_2-OH groups. Recently, it has been shown that thermal activation of MIL-47(V^{III})-AS under vacuum can lead to the LP form of MIL-47, in which the vanadium atoms are still in a +III oxidation state.[15] The specially activated LP form of MIL-47(V^{III}) material still bears μ_2-OH groups and thus can transform into a hydrated narrow pore (NP) form upon cooling to room temperature. More recently, the LP form of MIL-47(V^{IV}) has also been shown to change to a NP form under high mechanical pressure.[16] It is interesting to note that such framework flexibility has formerly been observed and intensively studied for the MIL-53 series of compounds [M^{III}(OH)(BDC)]·n(guests) (M = Al, Cr, Ga, Fe)[17] that bears the same framework topology as that of MIL-47. Because of these unique structural, sorption, and thermal features, MIL-47 has been the subject of a wide variety of applications such as catalysis,[18] and adsorption and separation of gases[19,20] and liquids.[21,22]

Our research group has made efforts in the preparation of vanadium-based MOFs because of their promising applications in adsorption[23,24] and heterogeneous catalysis.[18] Very recently, we have reported the remarkable gas (N_2 and CO_2) adsorption properties of vanadium analogues of nonfunctionalized and amino-functionalized MOFs having MIL-101 topology.[23] We have explored the outstanding heterogeneous catalytic performance of vanadium-based MIL-47 with low leaching in the oxidation of cyclohexene using *tert*-butyl hydroperoxide as an oxidant.[18] Recently, our group has reported the preparation and heterogeneous catalytic activity of a new vanadium 2,6-naphthalenedicarboxylate (NDC), [V^{IV}(OH)(NDC)] (denoted as COMOC-3) in cyclohexene epoxidation.[25] More recently, we have investigated the breathing behavior of a novel vanadium biphenyl-4,4′-dicarboxylate (BPDC), [V^{IV}(OH)-(BPDC)] (denoted as COMOC-2) upon adsorption of N_2, CO_2, and *n*-hexane.[24]

Encouraged by the above-mentioned properties and applications of vanadium-based MOFs, specifically those of MIL-47, we have introduced six different functional groups (electron withdrawing, −Cl, −Br, $-CF_3$; electron donating, $-CH_3$, −OH, $-OCH_3$) into the parent MIL-47(V^{IV}) framework to evaluate the effect of such organic functionalities (Scheme 1) on the sorption property and thermal stability of

Scheme 1. Functionalized Terephthalic Acid Linker Molecules H_2BDC-X Used for Preparing MIL-47(V^{IV})-X Compounds

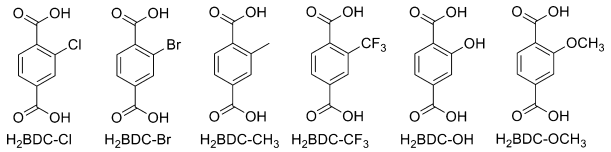

the resulting solids. Although a series of isotypic MIL-47(V^{IV})-X (X = $-C_4H_4$, $-(OH)_2$, $-(CH_3)_2$, $-Cl_4$, and $-Br_4$) compounds has previously been reported,[26] their sorption behavior has not been investigated.

Recently, Llewellyn and co-workers emphasized the importance of MIL-47 compared to other MOFs for CO_2 adsorption and CO_2/CH_4 separation.[27] Among the studied MOF-materials, MIL-47 was found to have the highest working capacity between 1 and 6 bar at 303 K. These are typical conditions for pressure swing adsorption (PSA), which is a technology used to separate some gases from a mixture of gases. With operando infrared experiments, they could characterize the strength of the microscopic interactions in play and found an adsorption enthalpy around −27.6 kJ/mol, which is similar to the values obtained via microcalorimetry (−20 to −25 kJ/mol).[19] This relatively weak enthalpy of adsorption suggests that no specific adsorption sites are present in the MIL-47 sample for the CO_2 quadrupole to interact with. Using functionalized linkers (Scheme 1), we can expect that the working capacity will increase further.

Ab initio as well as molecular mechanics simulations have previously been used to investigate the sorption properties of MIL-47. On one hand, periodic DFT calculations were used to verify the adsorption behavior of CO_2 in MIL-47(V^{IV}). The major conclusion was that there are no preferential adsorption sites for CO_2.[28] On the other hand, grand canonical Monte Carlo (GCMC) simulations were applied to study the adsorption mechanism and corresponding CO_2 adsorption isotherms.[29,30] Such GCMC techniques typically require atomic charges (mostly extracted from periodic DFT calculations) and interatomic potentials (often Lennard-Jones type) to describe the adsorbate−host interactions. Note that several studies have already reported GCMC simulations of various adsorbates on MIL-47: H_2,[31] N_2,[29] CO_2,[32] CH_4,[20] alkanes,[33] benzene,[34] and xylenes.[35] In some of those studies, the one-component isotherms are typically computed to construct mixed compound isotherms[29,35] with the ideal adsorbed solution theory (IAST)[36,37] for the prediction of the separation behavior. For example, in the xylene separation study on MIL-47 of Castillo et al.,[35] the Henry coefficients and low coverage heats of adsorption and adsorption entropies were computed at 543 K, and they showed an excellent agreement

dx.doi.org/10.1021/jp406835n | J. Phys. Chem. C 2013, 117, 22784−22796

with experiments. Furthermore, adsorption of xylene isomer mixtures could be modeled with IAST.

To our knowledge, no GCMC simulations with CO_2 on substituted MIL-47 materials have been reported in the literature. However, GCMC simulations have been used to describe adsorption phenomena of substituted MIL-47 and MIL-53 type materials.[38,39] Yu et al. studied adsorption phenomena of ammonia (NH_3) in a hierarchical modeling approach on four different MOFs (MIL-47, IRMOF-1, IRMOF-10, and IRMOF-16) modified with different functional groups (−OH, −C═O, −Cl, −COOH).[39] Hybrid Morse−Lennard-Jones potentials as well as Coulomb potentials were fitted using simulated annealing to match a large number of single-point MP2 energies at various distances and angles. The fitted potentials were then used in the GCMC simulations to predict ammonia adsorption isotherms and heats of adsorption in functionalized materials. More recently, Torrisi et al. studied the CO_2 adsorption in $(CH_3)_2$-, $(OH)_2$-, NH_2- and COOH-functionalized MIL-53(Al^{3+}) in its large pore form.[38] Ghysels et al. modeled the interplay between the breathing of the MIL-53(Al^{3+}) framework and the adsorption of CO_2 and CH_4.[40] In GCMC simulations and DFT calculations, it is generally accepted that framework confinement, defined by the pore structure and positions of the functional groups, plays a key role in characterizing the adsorption phenomena.

In this article, we wish to report the synthesis, complete characterization, and structural and sorption analysis of the above-mentioned functionalized MIL-47(V^{IV})-X solids (X = −Cl, −Br, $-CH_3$, $-CF_3$, −OH, $-OCH_3$). The structural, thermal, and sorption features of the compounds have been compared with the pristine MIL-47(V^{IV}). Furthermore, ab initio calculations on empty frameworks are combined with force-field Widom particle insertion simulations to gain more insight into the structural properties, flexibility, and exceptional CO_2 adsorption behavior of MIL-47(V^{IV})-OCH_3 as compared to that of the pure MIL-47(V^{IV}).

2. EXPERIMENTAL SECTION

2.1. Materials and General Methods. The $H_2BDC-Cl$, $H_2BDC-CH_3$, $H_2BDC-CF_3$, $H_2BDC-OH$ and $H_2BDC-OCH_3$ ligands were synthesized according to previously published procedures.[11,41−43] The synthesis procedures of the ligands and their ^1H NMR spectra are given in the Supporting Information. All other starting materials were of reagent grade and used as received from the commercial supplier. Weighing of VCl_3 was carried out in a nitrogen-filled glovebox. The calcined samples were also stored in the glovebox because of their air sensitivity. All other manipulations were carried out under an air atmosphere. Diffuse reflectance infrared Fourier transform (DRIFT) spectra were measured on a Thermo 6700 FLEX FTIR/FT-Raman instrument with a liquid nitrogen-cooled MCT-A (mercury−cadmium−tellurium) detector operating in a vacuum. The following indications are used to characterize absorption bands: very strong (vs), strong (s), medium (m), weak (w), shoulder (sh), and broad (br). Raman spectra were collected with an RXN1 Raman spectrometer (Kaiser Optical Systems) fitted with a 532 nm laser operating at 40 mW using an optical probe. Elemental analyses (C, H, N) were carried out on a Thermo Scientific Flash 2000 CHNS-O analyzer equipped with a TCD detector. Thermogravimetric analysis (TGA) was performed with a Netzsch STA-409CD thermal analyzer in a range of 25−600 °C under an air atmosphere at a heating rate of 2 °C min^{-1}. Ambient temperature X-ray powder diffraction (XRPD) patterns for all compounds except MIL-47(V^{III}) were recorded in an air atmosphere on a Thermo Scientific ARL X'Tra diffractometer operated at 40 kV, 40 mA using Cu Kα radiation (λ = 1.5406 Å). High-resolution synchrotron XRPD pattern for MIL-47(V^{III}) under vacuum was collected at beamline I11 of Diamond Light Source (Didcot, UK) using multianalyzing crystal-detectors (MACs) and a monochromatic beam with a wavelength of 0.827131 Å. The well-ground powder sample was filled in a 0.7 mm quartz capillary. Lattice parameters were determined using the DICVOL program.[44] Temperature-dependent XRPD patterns were collected with a Bruker D8 Discover X-ray diffractometer equipped with a linear detector; the XRD patterns were recorded from room temperature to 600 °C with a temperature ramp of 0.1 °C s^{-1} in air flow. The solution ^1H NMR spectra in d_6-DMSO were recorded on a Bruker AM 300 spectrometer at 300 MHz. The nitrogen sorption isotherms up to 1 bar were measured using a Belsorp Mini apparatus at −196 °C. The low-pressure carbon dioxide adsorption analyses were performed using a Micromeritics TriStar 3000 analyzer at 0 °C. The high-pressure carbon dioxide adsorption isotherms were recorded using a volumetric HPA 100 from VTI at 30 °C.

Syntheses. MIL-47(V^{IV}) was prepared according to a literature method.[14] The usual characterization experiments (XRPD, TGA, IR spectroscopy, and sorption analysis) were performed to confirm its purity. MIL-47(V^{III}) was prepared using a microwave-assisted method[26] as described below.

Synthesis of MIL-47(V^{III})-AS. A mixture of VCl_3 (100 mg, 0.64 mmol) and H_2BDC (106 mg, 0.64 mmol) in 2 mL of water was placed in a Pyrex tube (10 mL). The tube was sealed and heated in a microwave synthesizer (CEM, Discover S) to 170 °C at 150 W, held under these conditions for 30 min with stirring, and cooled to room temperature. The greenish yellow precipitate was collected by filtration and dried in air. The yield was 110 mg (0.33 mmol, 52%). Elemental analysis calcd for $C_{12.8}H_{8.6}O_{7.4}V$ (331.74 g mol^{-1}), C 38.79, H 1.74; found, C 38.30, H 1.52%. DRIFT (KBr, cm^{-1}): 3609 (br), 2661 (br), 2537 (br), 1704 (s), 1559 (vs), 1511 (m), 1427 (sh), 1400 (vs), 1285 (s), 1136 (w), 1018 (m), 911 (br), 824 (w), 776 (w), 744 (s), 731 (sh).

Synthesis of MIL-47(V^{III})-Cl-AS. This compound was obtained as a greenish yellow powder by the procedure described for MIL-47-AS, except the linker used was $H_2BDC-Cl$ (128 mg, 0.64 mmol) instead of H_2BDC. The yield was 135 mg (0.39 mmol, 58%). Elemental analysis calcd for $C_{11.2}H_6Cl_{1.4}O_{6.6}V$ (346.74 g mol^{-1}), C 38.79, H 1.74; found, C 38.30, H 1.52%. DRIFT (KBr, cm^{-1}): 3594 (m), 2652 (br), 2530 (br), 1819 (w), 1703 (s), 1571 (vs), 1489 (s), 1401 (vs), 1289 (s), 1255 (sh), 1159 (w), 1129 (w), 1050 (m), 976 (sh), 911 (s), 860 (sh), 830 (w), 778 (sh), 762 (s), 748 (sh), 707 (w), 683 (w), 670 (w).

Synthesis of MIL-47(V^{III})-Br-AS. This compound was obtained as a greenish yellow powder by the procedure described for MIL-47-AS, except the linker used was $H_2BDC-Br$ (156 mg, 0.64 mmol) instead of H_2BDC. The yield was 140 mg (0.36 mmol, 57%). Elemental analysis calcd for $C_{10.4}H_{5.5}Br_{1.3}O_{6.2}V$ (384.47 g mol^{-1}), C 32.49, H 1.44; found, C 32.30, H 1.32%. DRIFT (KBr, cm^{-1}): 3591 (m), 2649 (br), 2533 (br), 1700 (s), 1567 (vs), 1478 (s), 1400 (vs), 1290 (s), 1252 (sh), 1160 (w), 1130 (w), 1041 (s), 976 (sh), 915 (s), 863 (sh), 829 (w), 761 (s), 730 (w), 693 (w), 662 (w).

dx.doi.org/10.1021/jp406835n | J. Phys. Chem. C 2013, 117, 22784−22796

Synthesis of MIL-47(V^{III})-CH_3-AS. This compound was obtained as a greenish yellow powder by the procedure described for MIL-47-AS, except the linker used was $H_2BDC-CH_3$ (115 mg, 0.64 mmol) instead of H_2BDC. The yield was 105 mg (0.35 mmol, 55%). Elemental analysis calcd for $C_{11.7}H_{9.4}O_{6.2}V$ (300.13 g mol^{-1}), C 46.82, H 3.15; found, C 48.40, H 3.32%. DRIFT (KBr, cm^{-1}): 3600 (m), 2657 (br), 2530 (br), 1697 (s), 1550 (vs), 1413 (vs), 1381 (s), 1299 (s), 1268 (sh), 1201 (m), 1163 (w), 1133 (w), 1102 (w), 1082 (w), 1031 (w), 977 (sh), 909 (s), 861 (sh), 827 (w), 784 (w), 756 (s), 685 (w).

Synthesis of MIL-47(V^{III})-CF_3-AS. This compound was obtained as a greenish yellow powder by the procedure described for MIL-47-AS, except the linker used was $H_2BDC-CF_3$ (149 mg, 0.64 mmol) instead of H_2BDC. The yield was 120 mg (0.35 mmol, 55%). Elemental analysis calcd for $C_{12.6}H_6F_{4.2}O_{6.6}V$ (393.71 g mol^{-1}), C 38.43, H 1.53; found, C 38.40, H 1.32%. DRIFT (KBr, cm^{-1}): 3624 (m), 1560 (vs), 1500 (m), 1418 (sh), 1398 (vs), 1298 (s), 1178 (sh), 1150 (s), 1128 (sh), 1050 (m), 929 (m), 909 (sh), 834 (w), 768 (m), 705 (w), 664 (w).

Synthesis of MIL-47(V^{III})-OH-AS. This compound was obtained as a greenish yellow powder by the procedure described for MIL-47-AS, except the linker used was $H_2BDC-OH$ (116 mg, 0.64 mmol) instead of H_2BDC. The yield was 95 mg (0.30 mmol, 49%). Elemental analysis calcd for $C_{10.4}H_{7.4}O_{7.8}V$ (308.10 g mol^{-1}), C 40.54, H 2.42; found, C 40.40, H 2.32%. DRIFT (KBr, cm^{-1}): 3590 (m), 2649 (br), 2535 (br), 1698 (s), 1561 (vs), 1500 (s), 1400 (vs), 1290 (s), 1246 (s), 1219 (sh), 1159 (w), 1125 (w), 1049 (m), 965 (sh), 911 (s), 838 (w), 797 (w), 767 (s), 710 (w), 697 (w), 670 (w).

Synthesis of MIL-47(V^{III})-OCH_3-AS. This compound was obtained as a greenish yellow powder by the procedure described for MIL-47-AS, except the linker used was $H_2BDC-OCH_3$ (125 mg, 0.64 mmol) instead of H_2BDC. The yield was 95 mg (0.32 mmol, 50%). Elemental analysis calcd for $C_{10.8}H_{8.6}O_7V$ (301.32 g mol^{-1}), C 43.04, H 2.87; found, C 43.40, H 2.62%. DRIFT (KBr, cm^{-1}): 3572 (br), 3201 (br), 1702 (s), 1641 (m), 1616 (m), 1546 (s), 1505 (s), 1450 (sh), 1420 (vs), 1385 (sh), 1295 (s), 1244 (vs), 1219 (sh), 1159 (w), 1093 (w), 1023 (m), 962 (m), 897 (m), 836 (m), 801 (w), 771 (vs), 695 (w).

Activation of MIL-47(V^{III})-X-AS Compounds. A suspension of each (0.5 g) of MIL-47(V^{III})-Cl-AS and MIL-47(V^{III})-OCH_3-AS in DMF (30 mL) was heated at 150 °C for 5 h in an oil bath. The filtered solids were heated (320 °C, MIL-47(V^{III})-AS; 280 °C, MIL-47(V^{III})-OCH_3-AS) under dynamic vacuum for 24 h to get the activated forms of the compounds.

Each (0.5 g) of MIL-47(V^{III})-Br-AS, MIL-47(V^{III})-CH_3-AS, MIL-47(V^{III})-CF_3-AS, MIL-47(V^{III})-OH-AS and MIL-47(V^{III})-AS (synthesized using microwave irradiation) was directly heated (300 °C, 24 h, MIL-47(V^{III})-Br-AS; 300 °C, 24 h, MIL-47(V^{III})-CH_3-AS; 330 °C, 12 h, MIL-47(V^{III})-CF_3-AS; 280 °C, 24 h, MIL-47(V^{III})-OH-AS; MIL-47(V^{III})-AS, 330 °C, 12 h) under dynamic vacuum to obtain the evacuated forms of the compounds. Using this activation procedure, MIL-47(V^{III}) sample was obtained.

The MIL-47(V^{III})-AS sample, synthesized using conventional electric heating, was calcined at 300 °C for 21.5 h in an air atmosphere to get MIL-47(V^{IV}).

2.2. Results and Discussion. *Syntheses and Activation.* Similar and rapid microwave-assisted hydrothermal conditions (170 °C, 30 min, 150 W) have been employed to synthesize all six functionalized compounds and the unfunctionalized one, starting from an aqueous reaction mixture of VCl_3 and BDC-X linker present in a molar ratio of 1:1. It is worth noting that the microwave irradiation route has been formerly applied to synthesize five isostructural and functionalized MIL-47(V^{IV})-X (X = $-C_4H_4$, $-(OH)_2$, $-(CH_3)_2$, $-Cl_4$, and $-Br_4$) compounds.[26] Following the literature procedure, we have also synthesized MIL-47(V^{IV}) using conventional electric heating under hydrothermal conditions.[14]

The AS-forms of all the compounds contain guest molecules (H_2BDC-X linkers or H_2O) encapsulated in the pores which were removed by direct thermal treatment (MIL-47(V^{III})-Br-AS, MIL-47(V^{III})-CH_3-AS, MIL-47(V^{III})-CF_3-AS, and MIL-47(V^{III})-OH-AS) under vacuum or in a two-step procedure (MIL-47(V^{III})-Cl-AS and MIL-47(V^{III})-OCH_3-AS). For the latter two compounds, the guest molecules were exchanged by heating the AS compounds with a polar solvent such as *N,N′*-dimethylformamide (DMF). In a second step, the DMF molecules were removed by heating the guest-exchanged compounds under dynamic vacuum. The MIL-47(V^{III})-AS sample, which was prepared using conventional electric heating, was further heated in air to obtain the empty-pore form MIL-47(V^{IV}). On the other hand, the MIL-47(V^{III})-AS sample, which was synthesized using microwave irradiation, was subjected to thermal activation under vacuum in order to get the evacuated form MIL-47(V^{III}). For the functionalized MIL-47(V^{III})-X-AS samples, the thermal treatment under vacuum led to the empty-pore forms MIL-47(V^{IV})-X (cf. DRIFT and Raman Analysis).

DRIFT and Raman Analysis. The DRIFT spectra of the AS and empty-pore forms of each of the isostructural MIL-47-X compounds (Figure 2 and Figure S1 of the Supporting Information) are similar, as expected. In the DRIFT spectra of AS forms of all six compounds, the strong absorption bands due to asymmetric and symmetric $-CO_2$ stretching vibrations of the coordinated terephthalate linker molecules are located in the 1542−1566 cm^{-1} and 1393−1420 cm^{-1} regions, respectively.[10] The additional strong absorption bands in the 1695−1708 cm^{-1} region, observed in the DRIFT spectra of AS forms of the compounds, can be attributed to the protonated form ($-CO_2H$) of unreacted or occluded BDC-X linkers.[45] The intensity of absorption bands of the noncoordinated H_2BDC-X molecules are significantly reduced in the DRIFT

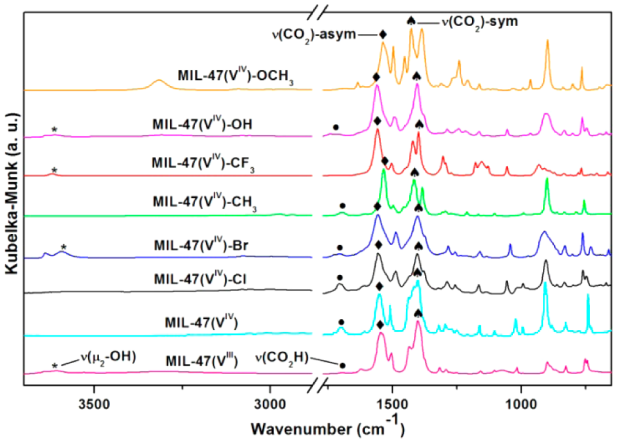

Figure 2. DRIFT spectra of MIL-47(V^{IV})-X and MIL-47(V^{IV}) measured under vacuum.

dx.doi.org/10.1021/jp406835n | J. Phys. Chem. C 2013, 117, 22784−22796

spectra of empty-pore forms of the compounds, suggesting almost complete activation. The C−H stretching frequency of the $-CH_3$ group attached with the BDC−CH_3 linker displays weak absorption bands at ca. 2541 and 2653 cm^{-1} in the DRIFT spectra of AS and empty-pore forms of MIL-47-CH_3.[46] The stretching vibration of the μ_2-OH group (Figure S1 of the Supporting Information) exhibits medium absorption bands in the DRIFT spectra of AS forms of the compounds.[11] These bands are almost completely absent (MIL-47(V^{IV})-Br, MIL-47(V^{IV})-CF_3, MIL-47(V^{IV})-OH, and MIL-47(V^{IV})-OCH_3) or significantly reduced in intensity (MIL-47(V^{IV})-Cl and MIL-47(V^{IV})-CH_3) in the DRIFT spectra (Figure 2) of the empty-pore forms of the compounds.

Raman analyses (Figure 3) were carried out to determine the oxidation state of the vanadium atoms in the thermally activated solids. Like the DRIFT spectra, the Raman spectra of the empty-pore forms of each of the structurally related MIL-47-X compounds are expectedly similar. The stretching vibration of the V^{IV}═O group is observed at ca. 900 cm^{-1} for all the compounds, except the MIL-47 sample, for which thermal activation was carried out under vacuum. Thus, similar thermal activation under vacuum led to different oxidation states for the vanadium atoms (+III for MIL-47, whereas +IV for MIL-47-X). It is worth noting that the LP form of MIL-47(V^{III}) has formerly been obtained by thermal activation under vacuum.[15] Note that the amplitude of the Raman intensity is higher for the pristine MIL-47 materials because these materials were synthesized in larger quantities and hence larger amounts of samples were used for the Raman analysis.

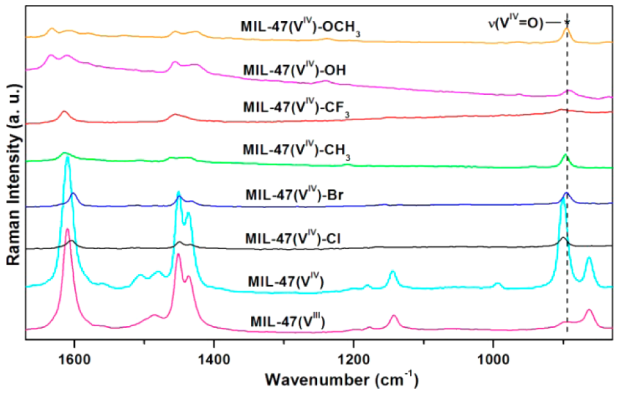

Figure 3. Raman spectra of MIL-47(V^{IV})-X and MIL-47(V^{IV}) measured under vacuum.

Structure Description. The refined lattice parameters (Table 1) of the filled (AS) and empty-pore forms of the MIL-47-X compounds determined from their room-temperature XRPD patterns are similar to the unfunctionalized MIL-47 exhibiting an orthorhombic structure (Figure 1). The different forms of the presented MIL-47-X compounds are thus isostructural with MIL-47, which is also revealed from the similarity between their XRPD patterns (Figure 4 and Figures S2 and S3 of the Supporting Information). As described by Férey's group,[14] the structure of MIL-47(V^{III})-AS contains infinite tilted *trans* chains (Figure 1) of corner-sharing (via μ_2-OH group) [$V^{III}O_4(OH)_2$] octahedra, which are interconnected by the carboxylate groups of the BDC linkers to form a three-dimensional (3D) framework possessing one-dimensional (1D) rhombic-shaped pores. In the AS-forms of the functionalized compounds, the 1D channels are occupied by guest molecules (solvent molecules or H_2BDC-X linkers) at ambient conditions. The guest molecules are removed by thermal activation leading to

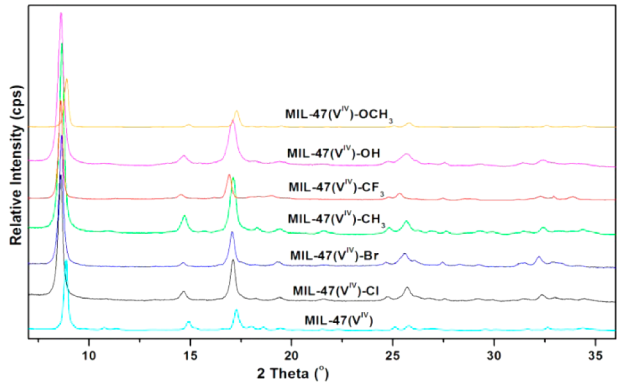

Figure 4. Experimental XRPD patterns (λ = 1.5406 Å) of MIL-47(V^{IV})-X and MIL-47(V^{IV}) measured in an air atmosphere.

Table 1. Molecular Formulae and Refined Lattice Parameters[a] of the Different Forms of the MIL-47-X Compounds

compound	molecular formula	*a* (Å)	*b* (Å)	*c* (Å)	*V* (Å^3)
MIL-47(V^{III})-Cl-AS	[V^{III}(OH)(BDC−Cl)]·0.4(H_2BDC-Cl)	16.84(3)	13.159(13)	6.921(6)	1534.0(40)
MIL-47(V^{III})-Br-AS	[V^{III}(OH)(BDC−Br)]·0.3(H_2BDC−Br)	16.716(14)	13.493(15)	6.939(6)	1565.2(29)
MIL-47(V^{III})-CH_3-AS	[V^{III}(OH)(BDC−CH_3)]·0.3(H_2BDC−CH_3)	16.811(22)	13.407(20)	6.959(7)	1568.5(46)
MIL-47(V^{III})-CF_3-AS	[V^{III}(OH)(BDC−CF_3)]·0.4(H_2BDC−CF_3)	15.64(3)	13.08(5)	7.154(14)	1463.1(97)
MIL-47(V^{III})-OH-AS	[V^{III}(OH)(BDC−OH)]·0.3(H_2O) 0.3(H_2BDC−OH)	17.01(4)	12.969(21)	6.908(8)	1524.4(57)
MIL-47(V^{III})-OCH_3-AS	[V^{III}(OH)(BDC−CH_3)]·0.2(H_2BDC−OCH_3)	16.89(4)	12.947(21)	6.887(10)	1506.4(78)
MIL-47(V^{III})-AS	[V^{III}(OH)(BDC)]·0.6(H_2BDC)	17.719(14)	12.143(5)	7.098(19)	1527.45(32)
MIL-47(V^{IV})-Cl	[V^{IV}(O)(BDC−Cl)]	16.49(4)	13.51(3)	6.830(10)	1521.3(47)
MIL-47(V^{IV})-Br	[V^{IV}(O)(BDC−Br)]	16.572(14)	13.619(15)	6.881(5)	1553.0(28)
MIL-47(V^{IV})-CH_3	[V^{IV}(O)(BDC−CH_3)]	16.42(4)	13.612(13)	6.838(6)	1528.8(47)
MIL-47(V^{IV})-CF_3	[V^{IV}(O)(BDC−CF_3)]	15.980(6)	14.212(7)	6.901(6)	1567.2(21)
MIL-47(V^{IV})-OH	[V^{IV}(O)(BDC−OH)]	16.67(3)	13.492(23)	6.834(5)	1537.5(42)
MIL-47(V^{IV})-OCH_3	[V^{IV}(O)(BDC−OCH_3)]	16.222(25)	13.79(3)	6.797(11)	1520.3(45)
MIL-47(V^{III})	[V^{III}(O)(BDC)]	16.440(7)	13.815(3)	6.886(14)	1564.0(27)
MIL-47(V^{IV})	[V^{IV}(O)(BDC)]	17.434(7)	13.433(3)	6.620(20)	1550.67(29)

[a]The lattice parameters of all the compounds correspond to an orthorhombic unit cell.

dx.doi.org/10.1021/jp406835n | J. Phys. Chem. C 2013, 117, 22784−22796

the empty-pore forms of the compounds. During thermal activation (in air for MIL-47 and under vacuum for MIL-47-X), the framework V^{3+} ions are oxidized to V^{4+} and the V−OH bonds are changed to a vanadyl (V═O) group, but the topology of the framework remains unchanged. In contrast, thermal activation under vacuum led MIL-47, in which the vanadium atoms still retain their +III oxidation state. Taking into account the van der Waals radii of the O atoms, the pore dimensions of the filled and empty-pore forms of MIL-47 are 11.6 × 6.8 Å and 10.6 × 8.8 Å, respectively. The unit cell volumes of MIL-47-X(V^{III})-AS and MIL-47(V^{IV})-X (Table 1) lie in the ranges 1463.1(97)−1568.5(46) and 1520.3(45)−1567.2(21) Å, respectively. The unit cell volumes of MIL-47(V^{III})-AS (1472.0(20) Å) and the empty-pore forms of MIL-47(V^{III}) (1564.0(27) Å) and MIL-47(V^{IV}) (1557.0(15) Å) lie within the above two ranges. Thus, the evacuated MIL-47 structures in both +III and +IV oxidation states exhibit LP forms similar to the AS forms. The LP form of MIL-47(V^{III}) compound has recently been obtained under similar activation conditions.[15] The specially activated MIL-47(V^{III}) still bears μ_2-OH groups and thus can transform into a hydrated NP form upon cooling to room temperature.

Thermal Stability. To examine the thermal stability of all MIL-47-X compounds, thermogravimetric analyses (TGA) were performed in an air atmosphere. On the basis of the TGA analyses, all the compounds are thermally stable up to 330−385 °C. The descending order of thermal stability of the compounds is MIL-47(V^{III})-Br-AS (385 °C) > MIL-47(V^{III})-CF_3-AS (380 °C) > MIL-47(V^{III})-Cl-AS (370 °C) > MIL-47(V^{III})-OCH_3-AS (360 °C) > MIL-47(V^{III})-CH_3-AS (350 °C) > MIL-47(V^{III})-OH-AS (330 °C). The highest thermal stability of MIL-47(V^{III})-Br-AS (385 °C) is close to that of the nonmodified MIL-47(V^{III})-AS compound (400 °C).[14]

In the TGA curves of the AS forms of all the compounds (Figure 5), any weight loss step that occurs below the decomposition temperature of the frameworks can be assigned to the removal of the occluded guest molecules (H_2O or H_2BDC-X linkers). The observed weight losses of the AS forms are consistent with the calculated ones as well as the elemental analyses (Tables S1 and S2 of the Supporting Information), indicating phase purity of the compounds.

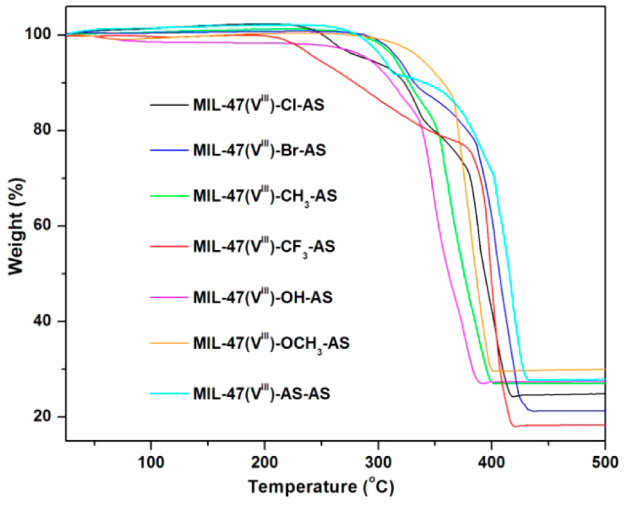

Figure 5. TGA curves of MIL-47(V^{III})-Cl-AS (black), MIL-47(V^{III})-Br-AS (blue), MIL-47(V^{III})-CH_3-AS (green), MIL-47(V^{III})-CF_3-AS (red), MIL-47(V^{III})-OH-AS (magenta), MIL-47(V^{III})-OCH_3-AS (orange), and MIL-47(V^{III})-AS (cyan) recorded in an air atmosphere.

The high thermal stability of the MIL-47(V^{III})-X-AS compounds has also been verified by temperature-dependent XRPD (TDXRPD) measurements. According to the TDXRPD patterns (see Figure 6 for MIL-47(V^{III})-CH_3-AS and Figures

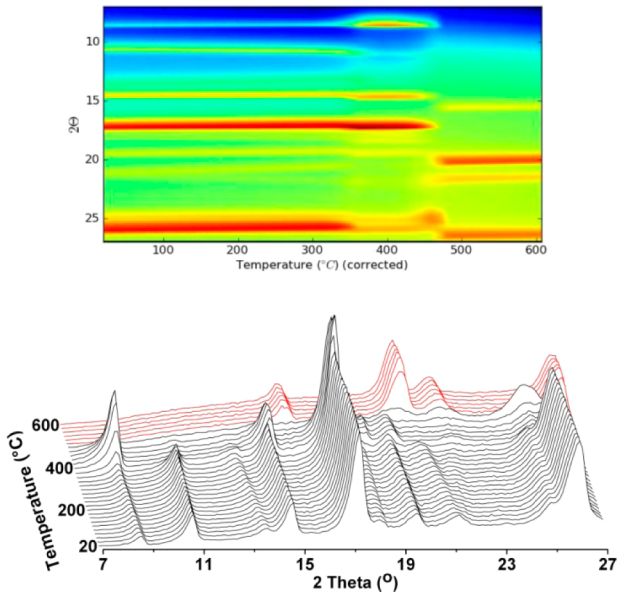

Figure 6. TDXRPD patterns (λ = 1.5406 Å) of MIL-47(V^{III})-CH_3-AS measured in an air atmosphere in the range of 20−600 °C. The black and red patterns denote stable and decomposed phases, respectively. The variation of the intensities of the Bragg peaks as a function of temperature is shown in the top panel.

S4−S8 of the Supporting Information for the other compounds), MIL-47(V^{III})-Cl-AS, MIL-47(V^{III})-Br-AS, MIL-47(V^{III})-CH_3-AS, MIL-47(V^{III})-CF_3-AS, MIL-47(V^{III})-OH-AS, and MIL-47(V^{III})-OCH_3-AS are stable up to 470, 485, 450, 480, 430, and 460 °C, respectively. The higher thermal stability obtained from TDXRPD measurements (6 °C min^{-1}) compared to TGA analyses (2 °C min^{-1}) is due to the faster heating rate used in the former measurement.

Sorption Properties. N_2 sorption measurements performed with the thermally activated MIL-47(V^{IV})-X compounds reveal type-I adsorption isotherms (Figure 7). The specific BET surface areas and micropore volumes (Table 2) derived from the N_2 adsorption isotherms exhibit considerable porosities, which are lower than those of the unfunctionalized MIL-47(V^{III}) and MIL-47(V^{IV}). Among the presented six functionalized compounds, MIL-47(V^{IV})-CH_3 adsorbs the highest amount of N_2. The N_2 uptake of MIL-47(V^{IV})-CH_3 is close to that of MIL-47(V^{IV}). It is worth noting that MIL-47(V^{III}) adsorbs slightly more N_2 than MIL-47(V^{IV}). The N_2 accessible specific BET surface areas decrease in the sequence MIL-47(V^{III}) > MIL-47(V^{IV}) > MIL-47(V^{IV})-CH_3 > MIL-47(V^{IV})-Cl > MIL-47(V^{IV})-CF_3 > MIL-47(V^{IV})-OCH_3 > MIL-47(V^{IV})-OH > MIL-47(V^{IV})-Br.

The low-pressure CO_2 adsorption isotherms (Figure 8) of the MIL-47-X compounds were recorded at 0 °C up to 1 bar. The decreasing order of the CO_2 uptake values (mmol g^{-1}) at 1 bar (i.e., p/p_0 = 0.3) is MIL-47(V^{IV})-OCH_3 (5.9) > MIL-47(V^{III}) (4.4) > MIL-47(V^{IV})-Cl (4.3) > MIL-47(V^{IV})-CH_3 (3.8) > MIL-47(V^{IV}) (3.4) > MIL-47(V^{IV})-CF_3 (3.0) > MIL-

dx.doi.org/10.1021/jp406835n | J. Phys. Chem. C 2013, 117, 22784−22796

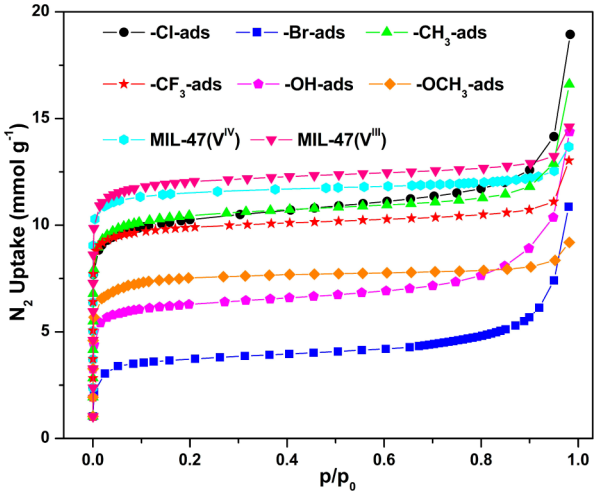

Figure 7. Low-pressure N_2 adsorption isotherms of MIL-47(V^{IV})-Cl (black, circles), MIL-47(V^{IV})-Br (blue, squares), MIL-47(V^{IV})-CH_3 (green, triangles), MIL-47(V^{IV})-CF_3 (red, stars), MIL-47(V^{IV})-OH (magenta, pentagons), MIL-47(V^{IV})-OCH_3 (orange, 45° rotated squares), MIL-47(V^{IV}) (cyan, hexagons) and MIL-47(V^{III}) (pink, upside down triangles) recorded at −196 °C.

Table 2. Specific BET Surface Areas and Micropore Volumes of the MIL-47(V^{IV})-X Compounds Determined from N_2 Adsorption Isotherms

compound	specific BET surface area[a] (m^2 g^{-1})	micropore volume[b] (cm^3 g^{-1})
MIL-47(V^{IV})-Cl	872	0.38
MIL-47(V^{IV})-Br	305	0.14
MIL-47(V^{IV})-CH_3	897	0.37
MIL-47(V^{IV})-CF_3	860	0.35
MIL-47(V^{IV})-OH	534	0.26
MIL-47(V^{IV})-OCH_3	637	0.27
MIL-47(V^{III})	1034	0.43
MIL-47(V^{IV})	997	0.38

[a]The specific BET surface areas have been calculated from the N_2 adsorption isotherms. [b]The micropore volumes have been calculated at p/p_0 = 0.5.

47(V^{IV})-Br (2.5). In comparison, the N_2 uptake values at p/p_0 = 0.3 follows the same trend as that of specific surface area. Thus, at p/p_0 = 0.3, the sequence of CO_2 uptake values does not match with that of N_2 uptake values. The CO_2 adsorption capacity of MIL-47(V^{IV})-OCH_3 at 1 bar and 0 °C is among the highest uptake values reported to date for MOFs.[47−50] The difference in CO_2 adsorption amounts among the MIL-47-X compounds should be attributed to the different functional groups attached to the terephthalate linkers, exerting various extents and nature of interactions with the CO_2 molecules. In addition, the oxidation state of the vanadium atoms and thus the presence or absence of μ_2-OH groups in the framework seem to play an important role in determining the CO_2 uptake values, as exemplified by the different amounts of CO_2 adsorbed by MIL-47(V^{III}) and MIL-47(V^{IV}). It is worth noting that the decrease in effective pore size due to the attached functional groups might also result in a larger adsorption potential and therefore stronger CO_2 adsorption.

Encouraged by the high CO_2 adsorption capacity of MIL-47(V^{IV})-OCH_3 at 0 °C and 1 bar, we measured the CO_2 sorption isotherm of this compound at 30 °C up to 20 bar and compared the adsorption amount with that of MIL-47(V^{IV}) (Figure 9). Interestingly, the CO_2 uptake (mmol g^{-1}) of MIL-47(V^{IV})-OCH_3 (8.3) at 20 bar is higher than that of MIL-47(V^{IV}) (7.3) in spite of a significantly smaller BET surface area (637 versus 997 m^2 g^{-1}) between the two compounds. However, the CO_2 adsorption capacity of MIL-47(V^{IV})-OCH_3 is slightly lower than that of the literature value (10.5 mmol g^{-1})[19] for MIL-47(V^{IV}), demonstrating a dramatic enhancement of the CO_2 uptake by the −OCH_3 functional group, despite its bulkiness.

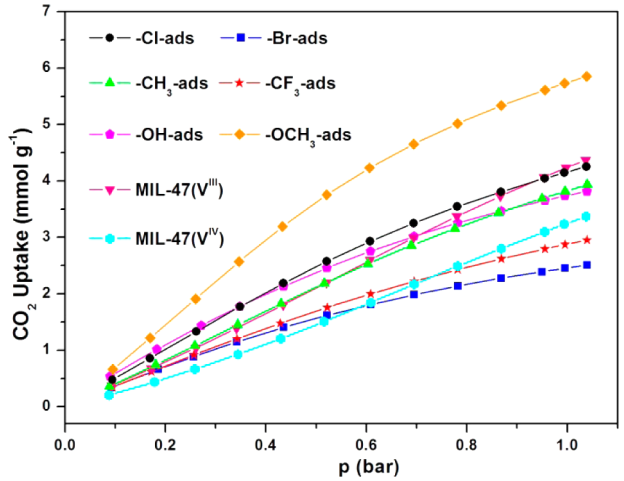

Figure 8. Low-pressure CO_2 adsorption isotherms of MIL-47(V^{IV})-Cl (black, circles), MIL-47(V^{IV})-Br (blue, squares), MIL-47(V^{IV})-CH_3 (green, triangles), MIL-47(V^{IV})-CF_3 (red, stars), MIL-47(V^{IV})-OH (magenta, pentagons), MIL-47(V^{IV})-OCH_3 (orange, 45° rotated squares), MIL-47(V^{IV}) (cyan, hexagons) and MIL-47(V^{III})-LP (upside down triangles, pink) recorded at 0 °C.

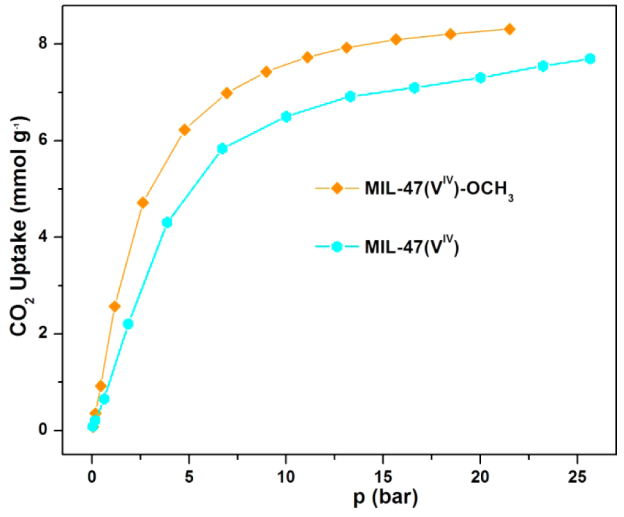

Figure 9. High-pressure CO_2 adsorption isotherms of the thermally activated MIL-47(V^{IV})-OCH_3 (orange, 45° rotated squares) and MIL-47(V^{IV}) (cyan, hexagons) measured at 30 °C.

3. COMPUTATIONAL RATIONALIZATION

3.1. Theoretical Methods. For the pristine MIL-47(V^{IV}) and the MIL-47(V^{IV})-OCH_3 structures, we have performed ab initio density functional theory (DFT) calculations within the

dx.doi.org/10.1021/jp406835n | J. Phys. Chem. C 2013, 117, 22784−22796

projector augmented wave (PAW) method as implemented in the Vienna ab initio Package (VASP) program using the generalized gradient approximation (GGA) functional as constructed by Perdew, Burke, and Ernzerhof (PBE).[51−54] The plane wave kinetic energy cutoff is set to 500 eV, and a Monkhorst−Pack special *k*-point grid of 3 × 3 × 3 *k*-points is used to sample the Brillouin zone.[55] Dispersive interactions, which play an important role in the flexibility of the crystal structure of MOFs, are included through the DFT-D3 method as implemented by Grimme et al., including Becke−Johnson damping.[56−59]

At this level the structures are modeled using a 72 and 88 atom super cell for MIL-47(V^{IV}) and MIL-47(V^{IV})-OCH_3, respectively. The theoretical calculations are limited to OCH_3 as substituent at the BDC linker in view of the high CO_2 uptake obtained experimentally. Because the actual relative position of the functional groups on different linkers is not known, and because of the high number of different combinations which can be constructed, we limit ourselves to two configurations, A and B, which are displayed in Figure 10. For the A configuration, all functional groups point into the same pore, resulting in the second pore being free of functional groups. Whereas for the B configuration there are two functional groups pointing inward for all pores. We expect that the properties of all other combinations are comparable to those found for the A and B configurations.

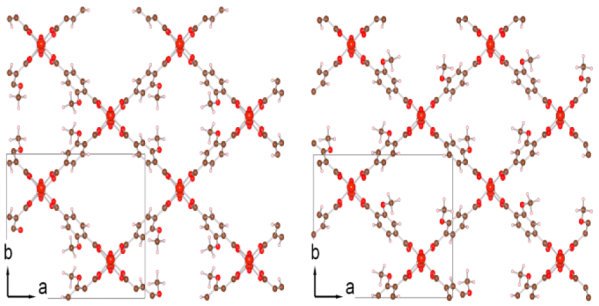

Figure 10. Ball-and-stick representation of a view along the pore direction of the A (left) and B (right) configurations for MIL-47(V^{IV})-OCH_3. A 2 × 2 supercell is shown, and the unit cell is indicated by the black rectangle. This figure was made with VESTA.[67]

We employed two different optimization routes. In both cases, the structures are optimized starting from an orthorhombic cell with the experimental lattice parameters. In the first case, all cell parameters (atomic positions, cell shape, and volume) are allowed to fully relax simultaneously, we will indicate these structures as "fully relaxed" (FR) structures. In the second case, only the atomic positions and the shape of the cell is allowed to change, while the volume is kept constant, preventing the cell from collapsing into a narrow pore geometry. We will refer to these structures as "fixed volume" (FV) structures. To optimize the structures, a conjugate gradient method is used. The convergence criterion is set to the difference in energy between subsequent steps becoming smaller than 1.0×10^{-6} eV. After full relaxation, the forces on the ions were found to be below 0.007 eV/Å.

The atomic charges of the systems are calculated using the iterative Hirshfeld-I approach[60,61] as implemented in our in-house developed code, HIVE.[62−64] Our implementation makes use of the grid-stored (pseudo) electron density distributions which are standardly obtained from VASP.[62,63] The atom-centered spherical integrations are done using Lebedev−Laikov grids of 1202 grid points per shell and a logarithmic radial grid.[65,66] The iterative scheme is considered converged when the largest difference in charge of a system atom is less than 1.0×10^{-5} electron in two consecutive iterations.

The Henry coefficients for the adsorption of CO_2 in MIL-47(V^{IV}) and MIL-47(V^{IV})-OCH_3 were estimated with the Widom particle insertion method.[68,69] These Henry coefficients describe the adsorption behavior in the low-pressure regime, which is the most relevant for selective CO_2 adsorption.[70] A complete simulation of the adsorption isotherms goes beyond the scope of this paper.

The interaction between the test particle (a CO_2 molecule) and the framework must be computed at least 10^9 times to get a statistically converged estimate of the Henry coefficient. Therefore, computationally efficient molecular mechanics force-fields are used. In this work, the interaction energy is modeled with an electrostatic and a van der Waals term. The electrostatic term is a simple point charge model, with Hirshfeld-I charges for the framework atoms and TraPPE charges for the CO_2 molecule.[71] For the van der Waals interactions, a Lennard-Jones model was used with UFF[72] parameters and a real-space cutoff of 10 Å. The Lorentz−Berthelot combination rules were used to derive framework−guest van der Waals parameters. In line with the TraPPE model, the CO_2 molecule has a rigid linear geometry with a CO bond length of 1.16 Å. Also, the framework geometry is fixed at the structures obtained with VASP. Note that subtle changes to this model, e.g., a different cutoff value, different van der Waals parameters for CO_2 (e.g., from the TraPPE model) or for the framework (e.g., from the DREIDING in ref 73), affect the magnitude of the Henry coefficients but not the ratios of the Henry coefficients for different structures. The current model was found to give a reasonable agreement with the experimental Henry coefficients for the MIL-47(V^{IV}) structure, and it is sufficient to provide insight into the observed trends. To obtain absolute quantitative theoretical predictions, more advanced approaches for the interactions between CO_2 and the framework are needed,[74,75] but these go beyond the scope of this work.

The interactions between the atoms of the CO_2 molecule and the empty framework are precomputed on uniform grids with a spacing of approximately 0.085 Å. During the Widom insertion computations, the interaction between CO_2 and the framework is derived from these grid data through trilinear interpolation. All force-field computations were carried out with Yaff, our in-house force-field simulation package.[76]

Usually, the Widom method involves a random sampling of the position and orientation of the test particle to compute the following thermodynamic average:

$$\exp(-\beta\mu_{ex}) = \int \exp[-\beta\mu(\mathbf{r}, \Omega)]\, d\mathbf{r}\, d\Omega$$

where μ_{ex} is the excess chemical potential, $\beta = 1/k_B T$, T = 273.15 K, and $U(\boldsymbol{r},\Omega)$ is the interaction energy of a single CO_2 test particle with the framework as function of its position ($\boldsymbol{r}$) and orientation (Ω). The integral is carried out over all possible positions and orientations of the CO_2 molecule in the framework. In this work, the position of the CO_2 molecule is sampled on a uniform grid and rotational degrees of freedom are sampled randomly. This enables a straightforward visualization of the local excess chemical potential, i.e.

dx.doi.org/10.1021/jp406835n | J. Phys. Chem. C 2013, 117, 22784−22796

$$\exp[-\beta\mu_{ex,local}(\mathbf{r})] = \int \exp[-\beta\mu(\mathbf{r}, \Omega)]\, d\Omega$$

through isosurfaces constructed from the uniform grid data. Preferential adsorption regions correspond to negative values of the local excess chemical potential. The theoretical Henry coefficient is derived from the excess chemical potential

$$K_H = \beta\exp(-\beta\mu_{ex})$$

To facilitate the comparison between the theoretical and experimental values, the value of K_H/ρ is reported in mmol g^{-1} bar^{-1}, where ρ is the framework density. The experimental value of K_H/ρ is simply computed as the slope of the line that connects the first data point of the adsorption isotherm with the origin.[77] In the zero-pressure limit, the isosteric heat of adsorption is computed as follows:

$$q_{is} = \frac{\partial \ln K_H}{\partial\beta} = \frac{1}{\beta} - \frac{\int U(\mathbf{r}, \Omega)\exp[-\beta U(\mathbf{r}, \Omega)]\, d\mathbf{r}\, d\Omega}{\int \exp[-\beta U(\mathbf{r}, \Omega)]\, d\mathbf{r}\, d\Omega}$$
$$= k_B T - \langle U\rangle$$

where $\langle U\rangle$ is the thermodynamic average of the interaction energy. The difference $\mu_{ex} - \langle U\rangle$ can be used to quantify the entropic penalty for the excess chemical potential due to the volume occupied by substituents or reduced pore volumes when a framework has collapsed.

3.2. Computational Results. After the relaxation, the FR MIL-47(V^{IV})-OCH_3 structures have collapsed into a narrow pore form, as shown in Table 3. The pure MIL-47(V^{IV}) structure, on the other hand, retained a large pore geometry, albeit with a volume that is slightly smaller than the experimentally observed value. The lattice parameter along the pore direction is in excellent agreement with the experimental value, making volume differences mainly the result of a change in the pore dimensions.

Table 3. Lattice Parameters and Volumes of the Optimized Theoretical Structures[a]

compound		a (Å)	b (Å)	c (Å)	V (Å^3)	ΔE (kJ mol^{-1})
MIL-47(V^{IV})	FR	16.685	13.437	6.789	1522.17	0.0
	FV	16.918	13.148	6.802	1513.11	0.4
MIL-47(V^{IV})-OCH_3 A	FR	18.510	10.380	6.792	1303.96	2.5
	FV	16.910	13.178	6.825	1520.50	0.0
MIL-47(V^{IV})-OCH_3 B	FR	18.336	10.701	6.774	1326.87	5.7
	FV	16.993	13.094	6.834	1520.50	4.6

[a]Relative energies of the structures are included. For each structure, the lowest in energy is used as a reference.

In case of the FV structures, all cells are slightly distorted from their initial orthorhombic cell shape, with variations of the cell angles up to 1.5° and lattice parameters within 5% of their initial experimental values.

An interesting aspect to note in these calculations is that the cell parameters of the MIL-47(V^{IV})-OCH_3 A and B configurations are roughly the same, i.e., the position of the functional groups seems to barely influence the crystal structure, in both the FR and FV case.

The theoretical relative energies of all structures are very small. Thermal corrections and typical errors on relative energies obtained with DFT-D3 computations lie in the same range[57] and may affect the relative stability of the structures. It is clear that all structures considered are energetically feasible and could occur simultaneously in experiment.

Table 4 shows the calculated Hirshfeld-I charges for all optimized crystal structures. The small differences in the charges are an indication of the good transferability of these Hirshfeld-I charges. Table 4 also reveals that roughly 1.41 electrons are transferred from the vanadium−oxygen chain to the organic linker, showing very good agreement with the expected formal charge of the linker. The influence of the functional group is shown to be very limited, and the resulting charge transfer is clearly localized on the linker itself.

Table 4. Average Atomic Charges As Calculated Using the Hirshfeld-I Scheme for the Vanadium Atoms (V), the Oxygen Atoms in the Vanadium−Oxygen Chain (O_{chain}), and the Total Charge of the Methoxy Group; Atomic Charges Are Given in Electrons

compound		V	O_{chain}	methoxy group
MIL-47(V^{IV})	FR	2.426	−1.012	−
	FV	2.425	−1.011	−
MIL-47(V^{IV})-OCH_3 A	FR	2.423	−1.008	−0.038
	FV	2.418	−1.004	−0.034
MIL-47(V^{IV})-OCH_3 B	FR	2.423	−1.012	−0.041
	FV	2.418	−1.005	−0.027

The results of the particle insertion computations are summarized in Table 5. The theoretical Henry coefficients are in qualitative agreement with the experimental results, except for the two FV structures of the MIL-47(V^{IV})-OCH_3 materials. In the FR forms of MIL-47(V^{IV})-OCH_3, a CO_2 molecule feels a significant additional interaction energy, $\langle U\rangle$, compared to MIL-47(V^{IV}). Hence, the entropic penalty in the excess chemical potential, $\mu_{ex} - \langle U\rangle$, due to the space occupied by the methoxy groups and the collapsed channels, is surmounted by approximately 3 kJ mol^{-1}. This leads to an increased Henry coefficient, K_H/ρ, for the FR forms. In the case of the FV structure, the minute extra binding seen in the average interaction energy, $\langle U\rangle$, is annihilated by entropic effects, leading to virtually no change in the Henry coefficient. These results suggest that at low CO_2 pressures, the MIL-47(V^{IV})-OCH_3 material should be in the collapsed form in order to observe the enhanced CO_2 affinity.

The mechanism for the enhanced CO_2 affinity is further clarified by the isosurfaces of the local excess chemical potential for MIL-47(V^{IV}) (FR), MIL-47(V^{IV})-OCH_3 A (FR), and MIL-47(V^{IV})-OCH_3 A (FV), shown in Figure 11. The gray and green isosurfaces correspond to a local excess chemical potential of 0 and −15 kJ mol^{-1}, respectively. The gray hulls indicate the regions that are accessible for the CO_2 guest molecules, while the green regions correspond to preferential binding volumes. Note that Figure 11a corresponds very well to the results of Torrisi obtained for MIL-53(Al).[38] In Figure 11b, the preferential binding region spans the entire accessible volume, leading to an enhanced CO_2 affinity. There are two potential contributions to the favorable binding of CO_2: (i) the electrostatic interaction between methoxy groups and the CO_2 and (ii) the stronger van der Waals interactions between the collapsed framework and the guest molecule. In Figure 11c,

dx.doi.org/10.1021/jp406835n | J. Phys. Chem. C 2013, 117, 22784−22796

Table 5. Results of the Widom Particle Insertion Simulations for the Different Structures Considered: Excess Chemical Potential (μ_{ex}), Isosteric Heat of Adsorption (q_{is}), Average Interaction Energy ($\langle U \rangle$), Entropic Penalty ($\mu_{ex} - \langle U \rangle$), and Theoretical and Experimental Henry Constants (K_H/ρ)

compound		μ_{ex} (kJ mol^{-1})	q_{is} (kJ mol^{-1})	$\langle U \rangle$ (kJ mol^{-1})	$\mu_{ex} - \langle U \rangle$ (kJ mol^{-1})	K_H/ρ (mmol g^{-1} bar^{-1}) theory	K_H/ρ (mmol g^{-1} bar^{-1}) experiment
MIL-47(V^{IV})	FR	−9.46	18.31	−16.04	6.58	2.81	2.34
	FV	−9.53	18.41	−16.14	6.61	2.89	2.34
MIL-47(V^{IV})-OCH$_3$ A	FR	−12.33	24.99	−22.72	10.39	7.54	6.99
	FV	−8.82	20.16	−17.89	9.16	1.88	6.99
MIL-47(V^{IV})-CH$_3$ B	FR	−12.72	25.37	−23.10	10.37	9.13	6.99
	FV	−9.23	20.40	−18.13	8.91	2.25	6.99

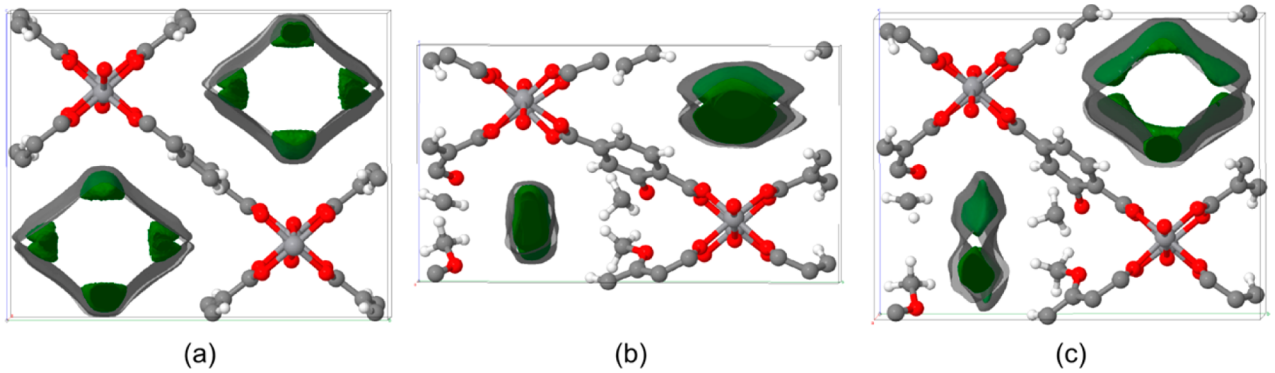

Figure 11. Local excess chemical potential isosurfaces for the structures (a) MIL-47(V^{IV}) (FR), (b) MIL-47(V^{IV})-OCH$_3$ A (FR), and (c) MIL-47(V^{IV})-OCH$_3$ A (FV). The gray and green isosurfaces correspond to a local excess chemical potential of 0 and −15 kJ mol^{-1}, respectively. This figure was made with JMol.[78]

only the effect of the substituent is accounted for as the unit cell volume is close to that of the pure MIL-47(V^{IV}). The binding regions decrease in size and are shapes that are similar to those in Figure 11a. These results show that both the presence of the methoxy group and the collapse of the MIL-47(V^{IV})-OCH$_3$ framework are driving the enhanced CO_2 affinity.

Given that the experimental Henry coefficient for the MIL-47(V^{IV})-OCH$_3$ structure lies between the theoretical predictions for the FR and FV form, it is reasonable to assume that structure partially collapses at low CO_2 pressure.

4. CONCLUSIONS

We have demonstrated the successful synthesis, complete characterization, and structural analysis of six new functionalized, isoreticular, redox-active, vanadium-based MOFs MIL-47-X (X = −Cl, −Br, −CH$_3$, −CF$_3$, −OH, −OCH$_3$). The phase purity of the compounds was confirmed by a combination of XRPD analysis, DRIFT spectroscopy, Raman, thermogravimetric and elemental analysis. TGA and temperature-dependent XRPD experiments show that the compounds possess high thermal stability (330−385) °C in an air atmosphere, which is comparable with that of unfunctionalized MIL-47. N_2 sorption measurements performed on the evacuated form of the compounds reveal significantly high uptakes (S_{BET} in the 305−897 m^2 g^{-1} range), which is dependent on the size of the attached functional groups. The CO_2 adsorption capacities of the compounds are dependent on both the size and the nature of attached functional groups (and thus the nature of framework-CO_2 interactions). MIL-47 bearing −OCH$_3$ functionality adsorbs the highest amount of CO_2 among the presented six functionalized compounds, and its CO_2 uptake value (5.9 mmol g^{-1}) at 0 °C and 1 bar is among the highest values reported so far. Finally, the redox activity of vanadium(III) atoms paired with the high thermal stability of the compounds in air would make the compounds useful in heterogeneous catalytic reactions.

Additional insights in structural properties and the adsorption of CO_2 in MIL-47(V^{IV}) and MIL-47(V^{IV})-OCH$_3$ were obtained from a computational analysis. We have performed ab initio DFT calculations on MIL-47(V^{IV}) and MIL-47(V^{IV})-OCH$_3$. For the pristine MIL-47(V^{IV}), an LP ground-state structure was found, while for the methoxy functionalized form, the narrow pore structure is most stable. However, because of the very flat energy landscape (only a few kilojoules per mole difference between LP and NP), both can be present in experimental samples at finite temperatures and pressures. For the MIL-47(V^{IV})-OCH$_3$ system it is found that the position of the functional group on the linkers has little to no influence on the crystal structure. Calculated atomic charges show that the methoxy group has only a very local influence on the electron distribution of the linker, with a charge-transfer from the linker to the methoxy group of less than 0.05 electron. Widom particle insertion simulations reveal two driving forces for the enhanced CO_2 affinity of the MIL-47(V^{IV})-OCH$_3$: (i) the presence of the substituents increases the adsorption enthalpy of CO_2 and (ii) the mildly collapsed structure of the framework allows a CO_2 molecule to interact simultaneously with all surrounding linkers and substituents.

■ ASSOCIATED CONTENT

Supporting Information

Additional ambient and temperature-dependent XRPD patterns and tables containing results of TG, DRIFT, and elemental analyses. This material is available free of charge via the Internet at http://pubs.acs.org.

dx.doi.org/10.1021/jp406835n | J. Phys. Chem. C 2013, 117, 22784−22796

AUTHOR INFORMATION

Corresponding Author

*E-mail: pascal.vandervoort@ugent.be. Tel: (+)32-964 4442. Fax: (+)32-92644983.

Notes

The authors declare no competing financial interest.

ACKNOWLEDGMENTS

The authors acknowledge the financial support from the Ghent University BOF Grants 01P02911T and 01D31608, GOA Grant 01G00710, and the Long Term Structural Methusalem Grant 01M00409. Diamond Light Source is acknowledged for providing access to the beamline I11. All calculations were carried out using the Stevin Supercomputer Infrastructure at Ghent University. T.V. is a postdoctoral researcher funded by the Foundation of Scientific Research−Flanders (FWO). V.V.S, M.V., and D.E.P.V. acknowledge the European Research Council for funding through the European Community's Seventh framework Programme (FP7(2007-2013) ERC GrantAgreement 240483). This research has been funded by the Interuniversity Attraction Poles Programme (P7/05) initiated by the Belgian Science Policy Office.

REFERENCES

(1) Ferey, G. Hybrid Porous Solids: Past, Present, Future. *Chem. Soc. Rev.* **2008**, *37*, 191−214.

(2) Li, J. R.; Kuppler, R. J.; Zhou, H. C. Selective Gas Adsorption and Separation in Metal-Organic Frameworks. *Chem. Soc. Rev.* **2009**, *38* (5), 1477−1504.

(3) Lee, J.; Farha, O. K.; Roberts, J.; Scheidt, K. A.; Nguyen, S. T.; Hupp, J. T. Metal-Organic Framework Materials as Catalysts. *Chem. Soc. Rev.* **2009**, *38*, 1450−1459.

(4) Horcajada, P.; Chalati, T.; Serre, C.; Gillet, B.; Sebrie, C.; Baati, T.; Eubank, J. F.; Heurtaux, D.; Clayette, P.; Kreuz, C.; et al. Porous Metal−Organic-Framework Nanoscale Carriers as a Potential Platform for Drug Delivery and Imaging. *Nat. Mater.* **2010**, *9*, 172−178.

(5) Tanabe, K. K.; Cohen, S. M. Postsynthetic Modification of Metal-Organic Frameworks − A Progress Report. *Chem. Soc. Rev.* **2011**, *40*, 498−519.

(6) Eddaoudi, M.; Kim, J.; Rosi, N.; Vodak, D.; Wachter, J.; O'Keeffe, M.; Yaghi, O. M. Systematic Design of Pore Size and Functionality in Isoreticular MOFs and Their Application in Methane Storage. *Science* **2002**, *295*, 469−472.

(7) Yang, C.; Wang, X. P.; Omary, M. A. Fluorous Metal−Organic Frameworks for High-Density Gas Adsorption. *J. Am. Chem. Soc.* **2007**, *129*, 15454−15455.

(8) Colombo, V.; Montoro, C.; Maspero, A.; Palmisano, G.; Masciocchi, N.; Galli, S.; Barea, E.; Navarro, J. A. R. Tuning the Adsorption Properties of Isoreticular Pyrazolate-Based Metal-Organic Frameworks through Ligand Modification. *J. Am. Chem. Soc.* **2012**, *134*, 12830−12843.

(9) Kandiah, M.; Nilsen, M. H.; Usseglio, S.; Jakobsen, S.; Olsbye, U.; Tilset, M.; Larabi, C.; Quadrelli, E. A.; Bonino, F.; Lillerud, K. P. Synthesis and Stability of Tagged UiO-66 Zr-MOFs. *Chem. Mater.* **2010**, *22*, 6632−6640.

(10) Biswas, S.; Ahnfeldt, T.; Stock, N. New Functionalized Flexible Al-MIL-53-X (X = -Cl, -Br, $-CH_3$, $-NO_2$, $-(OH)_2$) Solids: Syntheses, Characterization, Sorption, and Breathing Behavior. *Inorg. Chem.* **2011**, *50*, 9518−9526.

(11) Devic, T.; Horcajada, P.; Serre, C.; Salles, F.; Maurin, G.; Moulin, B.; Heurtaux, D.; Clet, G.; Vimont, A.; Greneche, J. M.; et al. Functionalization in Flexible Porous Solids: Effects on the Pore Opening and the Host−Guest Interactions. *J. Am. Chem. Soc.* **2010**, *132*, 1127−1136.

(12) Cavka, J. H.; Jakobsen, S.; Olsbye, U.; Guillou, N.; Lamberti, C.; Bordiga, S.; Lillerud, K. P. A New Zirconium Inorganic Building Brick Forming Metal Organic Frameworks with Exceptional Stability. *J. Am. Chem. Soc.* **2008**, *130*, 13850−13851.

(13) Ferey, G.; Mellot-Draznieks, C.; Serre, C.; Millange, F.; Dutour, J.; Surble, S.; Margiolaki, I. A Chromium Terephthalate-Based Solid with Unusually Large Pore Volumes and Surface Area. *Science* **2005**, *309*, 2040−2042.

(14) Barthelet, K.; Marrot, J.; Riou, D.; Ferey, G. A Breathing Hybrid Organic-Inorganic Solid with Very Large Pores and High Magnetic Characteristics. *Angew. Chem., Int. Ed.* **2002**, *41*, 281−284.

(15) Leclerc, H.; Devic, T.; Devautour-Vinot, S.; Bazin, P.; Audebrand, N.; Ferey, G.; Daturi, M.; Vimont, A.; Clet, G. Influence of the Oxidation State of the Metal Center on the Flexibility and Adsorption Properties of a Porous Metal Organic Framework: MIL-47(V). *J. Phys. Chem. C* **2011**, *115*, 19828−19840.

(16) Yot, P. G.; Ma, Q. T.; Haines, J.; Yang, Q. Y.; Ghoufi, A.; Devic, T.; Serre, C.; Dmitriev, V.; Ferey, G.; Zhong, C. L.; Maurin, G. Large Breathing of the MOF MIL-47(V^{IV}) Under Mechanical Pressure: A Joint Experimental-Modelling Exploration. *Chem. Sci.* **2012**, *3*, 1100−1104.

(17) Ferey, G.; Serre, C. Large Breathing Effects in Three-Dimensional Porous Hybrid Matter: Facts, Analyses, Rules and Consequences. *Chem. Soc. Rev.* **2009**, *38*, 1380−1399.

(18) Leus, K.; Vandichel, M.; Liu, Y. Y.; Muylaert, I.; Musschoot, J.; Pyl, S.; Vrielinck, H.; Callens, F.; Marin, G. B.; Detavernier, C.; et al. The Coordinatively Saturated Vanadium MIL-47 as a Low Leaching Heterogeneous Catalyst in the Oxidation of Cyclohexene. *J. Catal.* **2012**, *285*, 196−207.

(19) Bourrelly, S.; Llewellyn, P. L.; Serre, C.; Millange, F.; Loiseau, T.; Ferey, G. Different Adsorption Behaviors of Methane and Carbon Dioxide in the Isotypic Nanoporous Metal Terephthalates MIL-53 and MIL-47. *J. Am. Chem. Soc.* **2005**, *127*, 13519−13521.

(20) Rosenbach, N.; Ghoufi, A.; Deroche, I.; Llewellyn, P. L.; Devic, T.; Bourrelly, S.; Serre, C.; Ferey, G.; Maurin, G. Adsorption of Light Hydrocarbons in the Flexible MIL-53(Cr) and Rigid MIL-47(V) Metal-Organic Frameworks: A Combination of Molecular Simulations and Microcalorimetry/Gravimetry Measurements. *Phys. Chem. Chem. Phys.* **2010**, *12*, 6428−6437.

(21) Alaerts, L.; Kirschhock, C. E. A.; Maes, M.; van der Veen, M. A.; Finsy, V.; Depla, A.; Martens, J. A.; Baron, G. V.; Jacobs, P. A.; Denayer, J. F. M.; et al. Selective Adsorption and Separation of Xylene Isomers and Ethylbenzene with the Microporous Vanadium(IV) Terephthalate MIL-47. *Angew. Chem., Int. Ed.* **2007**, *46*, 4293−4297.

(22) Khan, N. A.; Jhung, S. H. Remarkable Adsorption Capacity of $CuCl_2$-Loaded Porous Vanadium Benzenedicarboxylate for Benzothiophene. *Angew. Chem., Int. Ed.* **2012**, *51*, 1198−1201.

(23) Biswas, S.; Couck, S.; Grzywa, M.; Denayer, J. F. M.; Volkmer, D.; Van der Voort, P. Vanadium Analogues of Nonfunctionalized and Amino-Functionalized MOFs with MIL-101 Topology − Synthesis, Characterization, and Gas Sorption Properties. *Eur. J. Inorg. Chem.* **2012**, 2481−2486.

(24) Liu, Y.-Y.; Couck, S.; Vandichel, M.; Grzywa, M.; Leus, K.; Biswas, S.; Volkmer, D.; Gascon, J.; Kapteijn, F.; Denayer, J. F. M.; Waroquier, M.; Van Speybroeck, V.; Van Der Voort, P. New V^{IV}-Based Metal−Organic Framework Having Framework Flexibility and High CO_2 Adsorption Capacity. *Inorg. Chem.* **2013**, *52*, 113−120.

(25) Liu, Y. Y.; Leus, K.; Grzywa, M.; Weinberger, D.; Strubbe, K.; Vrielinck, H.; Van Deun, R.; Volkmer, D.; Van Speybroeck, V.; Van der Voort, P. Synthesis, Structural Characterization, and Catalytic Performance of a Vanadium-Based Metal-Organic Framework (COMOC-3). *Eur. J. Inorg. Chem.* **2012**, 2819−2827.

(26) Centrone, A.; Harada, T.; Speakman, S.; Hatton, T. A. Facile Synthesis of Vanadium Metal-Organic Frameworks and their Magnetic Properties. *Small* **2010**, *6*, 1598−1602.

(27) Llewellyn, P. L.; Bourrelly, S.; Vagner, C.; Heymans, N.; Leclerc, H.; Ghoufi, A.; Bazin, P.; Vimont, A.; Daturi, M.; Devic, T.; et al. Evaluation of MIL-47(V) for CO_2-Related Applications. *J. Phys. Chem. C* **2013**, *117*, 962−970.

(28) Ramsahye, N. A.; Maurin, G.; Bourrelly, S.; Llewellyn, P. L.; Serre, C.; Loiseau, T.; Devic, T.; Ferey, G. Probing the Adsorption

Sites for CO_2 in Metal Organic Frameworks Materials MIL-53 (Al, Cr) and MIL-47 (V) by Density Functional Theory. *J. Phys. Chem. C* **2008**, *112*, 514−520.
(29) Liu, B.; Smit, B. Comparative Molecular Simulation Study of CO_2/N_2 and CH_4/N_2 Separation in Zeolites and Metal-Organic Frameworks. *Langmuir* **2009**, *25*, 5918−5926.
(30) Salles, F.; Jobic, H.; Devic, T.; Llewellyn, P. L.; Serre, C.; Ferey, G.; Maurin, G. Self and Transport Diffusivity of CO_2 in the Metal-Organic Framework MIL-47(V) Explored by Quasi-elastic Neutron Scattering Experiments and Molecular Dynamics Simulations. *ACS Nano* **2010**, *4*, 143−152.
(31) Salles, F.; Jobic, H.; Maurin, G.; Koza, M. M.; Llewellyn, P. L.; Devic, T.; Serre, C.; Ferey, G. Experimental Evidence Supported by Simulations of a Very High H_2 Diffusion in Metal Organic Framework Materials. *Phys. Rev. Lett.* **2008**, 100.
(32) Ramsahye, N. A.; Maurin, G.; Bourrelly, S.; Llewellyn, P. L.; Devic, T.; Serre, C.; Loiseau, T.; Ferey, G. Adsorption of CO_2 in Metal Organic Frameworks of Different Metal Centres: Grand Canonical Monte Carlo Simulations Compared to Experiments. *Adsorption* **2007**, *13*, 461−467.
(33) Deroche, I.; Rives, S.; Trung, T.; Yang, Q.; Ghoufi, A.; Ramsahye, N. A.; Trens, P.; Fajula, F.; Devic, T.; Serre, C.; Ferey, G.; Jobic, H.; Maurin, G. Exploration of the Long-Chain *N*-Alkanes Adsorption and Diffusion in the MOF-Type MIL-47 (V) Material by Combining Experimental and Molecular Simulation Tools. *J. Phys. Chem. C* **2011**, *115*, 13868−13876.
(34) Kolokolov, D. I.; Jobic, H.; Stepanov, A. G.; Ollivier, J.; Rives, S.; Maurin, G.; Devic, T.; Serre, C.; Ferey, G. Experimental and Simulation Evidence of a Corkscrew Motion for Benzene in the Metal-Organic Framework MIL-47. *J. Phys. Chem. C* **2012**, *116*, 15093−15098.
(35) Castillo, J. M.; Vlugt, T. J. H.; Calero, S. Molecular Simulation Study on the Separation of Xylene Isomers in MIL-47 Metal-Organic Frameworks. *J. Phys. Chem. C* **2009**, *113*, 20869−20874.
(36) Benjamin, M. M. New Conceptualization and Solution Approach for the Ideal Adsorbed Solution Theory (IAST). *Environ. Sci. Technol.* **2009**, *43*, 2530−2536.
(37) Myers, A. L.; Prausnitz, J. M. Thermodynamics of Mixed-Gas Adsorption. *AIChE J.* **1965**, *11*, 121−127.
(38) Torrisi, A.; Bell, R. G.; Mellot-Draznieks, C. Predicting the Impact of Functionalized Ligands on CO_2 Adsorption in MOFs: A Combined DFT and Grand Canonical Monte Carlo Study. *Microporous Mesoporous Mater.* **2013**, *168*, 225−238.
(39) Yu, D. C.; Ghosh, P.; Snurr, R. Q. Hierarchical Modeling of Ammonia Adsorption in Functionalized Metal-Organic Frameworks. *Dalton Trans.* **2012**, *41*, 3962−3973.
(40) Ghysels, A.; Vanduyfhuys, L.; Vandichel, M.; Waroquier, M.; Van Speybroeck, V.; Smit, B. On the Thermodynamics of Framework Breathing: A Free Energy Model for Gas Adsorption in MIL-53. *J. Phys. Chem. C* **2013**, *117*, 11540.
(41) Chen, Y. W.; Chen, L.; Zhou, W. H.; Zha, D. J.; Zhou, D.; Bai, F. L.; Wan, M. X. Synthesis and Properties of Polyacetylenes Containing Bis(4-alkylphenyl)terephthalate as Pendant and Methyleneoxy as Spacer. *Synth. Met.* **2009**, *159*, 1649−1656.
(42) Himsl, D.; Wallacher, D.; Hartmann, M. Improving the Hydrogen Adsorption Properties of a Hydroxy-Modified MIL-53(Al) Structural Analogue by Lithium Doping. *Angew. Chem., Int. Ed.* **2009**, *48*, 4639−4642.
(43) Kuwabara, M.; Murakami, A.; Fukunishi, K.; Nomura, M.; Yamanaka, H. Synthesis of Terephthalic Acids Containing Polyfluoroalkyl Groups. *J. Fluorine Chem.* **1989**, *42*, 105−118.
(44) Boultif, A.; Louer, D. Indexing of Powder Diffraction Patterns for Low-Symmetry Lattices by the Successive Dichotomy Method. *J. Appl. Crystallogr.* **1991**, *24*, 987−993.
(45) Loiseau, T.; Serre, C.; Huguenard, C.; Fink, G.; Taulelle, F.; Henry, M.; Bataille, T.; Ferey, G. A Rationale for the Large Breathing of the Porous Aluminum Terephthalate (MIL-53) upon Hydration. *Chem.—Eur. J.* **2004**, *10* (6), 1373−1382.
(46) Banwell, N.; McCash, E. M. *Fundamentals of Molecular Spectroscopy*; McGraw Hill: New York, 1994.
(47) Caskey, S. R.; Wong-Foy, A. G.; Matzger, A. J. Dramatic Tuning of Carbon Dioxide Uptake via Metal Substitution in a Coordination Polymer with Cylindrical Pores. *J. Am. Chem. Soc.* **2008**, *130*, 10870−10871.
(48) Park, J.; Li, J. R.; Chen, Y. P.; Yu, J. M.; Yakovenko, A. A.; Wang, Z. Y. U.; Sun, L. B.; Balbuena, P. B.; Zhou, H. C. A Versatile Metal-Organic Framework for Carbon Dioxide Capture and Cooperative Catalysis. *Chem. Commun.* **2012**, *48*, 9995−9997.
(49) Si, X. L.; Jiao, C. L.; Li, F.; Zhang, J.; Wang, S.; Liu, S.; Li, Z. B.; Sun, L. X.; Xu, F.; Gabelica, Z.; Schick, C. High and Selective CO_2 Uptake, H_2 Storage and Methanol Sensing on the Amine-Decorated 12-Connected MOF CAU-1. *Energy Environ. Sci.* **2011**, *4*, 4522−4527.
(50) Xiang, S. C.; He, Y. B.; Zhang, Z. J.; Wu, H.; Zhou, W.; Krishna, R.; Chen, B. L. Microporous Metal-Organic Framework with Potential for Carbon Dioxide Capture at Ambient Conditions. *Nat. Commun.* **2012**, *3*, 954−962.
(51) Blochl, P. E. Projector Augmented-Wave Method. *Phys. Rev. B: Condens. Matter Mater. Phys.* **1994**, *50* (24), 17953−17979.
(52) Kresse, G.; Furthmuller, J. Efficient iterative schemes for ab initio total-energy calculations using a plane-wave basis set. *Phys. Rev. B: Condens. Matter Mater. Phys.* **1996**, *54* (16), 11169−11186.
(53) Kresse, G.; Hafner, J. Ab Initio Molecular-Dynamics for Liquid-metals. *Phys. Rev. B: Condens. Matter Mater. Phys.* **1993**, *47* (1), 558−561.
(54) Kresse, G.; Joubert, D. From Ultrasoft Pseudopotentials to the Projector Augmented-Wave Method. *Phys. Rev. B: Condens. Matter Mater. Phys.* **1999**, *59*, 1758−1775.
(55) Monkhorst, H. J.; Pack, J. D. Special Points for Brillouin-Zone Integrations. *Phys. Rev. B: Condens. Matter Mater. Phys.* **1976**, *13*, 5188−5192.
(56) Grimme, S. Semiempirical GGA-Type Density Functional Constructed with a Long-Range Dispersion Correction. *J. Comput. Chem.* **2006**, *27*, 1787−1799.
(57) Grimme, S.; Antony, J.; Ehrlich, S.; Krieg, H. A Consistent and Accurate Ab Initio Parametrization of Density Functional Dispersion Correction (DFT-D) for the 94 Elements H-Pu. *J. Chem. Phys.* **2010**, *132*, 154104.
(58) Grimme, S.; Ehrlich, S.; Goerigk, L. Effect of the Damping Function in Dispersion Corrected Density Functional Theory. *J. Comput. Chem.* **2011**, *32*, 1456−1465.
(59) Walker, A. M.; Civalleri, B.; Slater, B.; Mellot-Draznieks, C.; Cora, F.; Zicovich-Wilson, C. M.; Roman-Perez, G.; Soler, J. M.; Gale, J. D. Flexibility in a Metal-Organic Framework Material Controlled by Weak Dispersion Forces: The Bistability of MIL-53(Al). *Angew. Chem., Int. Ed.* **2010**, *49*, 7501−7503.
(60) Bultinck, P. Critical Analysis of the Local Aromaticity Concept in Polyaromatic Hydrocarbons. *Faraday Discuss.* **2007**, *135*, 347−365.
(61) Bultinck, P.; Van Alsenoy, C.; Ayers, P. W.; Carbo-Dorca, R. Critical analysis and extension of the Hirshfeld atoms in molecules. *J. Chem. Phys.* **2007**, *126*, 144111-1−144111-9.
(62) Vanpoucke, D. E. P.; Bultinck, P.; Van Driessche, I. Extending Hirshfeld-I to Bulk and Periodic Materials. *J. Comput. Chem.* **2013**, *34*, 405−417.
(63) Vanpoucke, D. E. P.; Van Driessche, I.; Bultinck, P. Reply to 'Comment on "Extending Hirshfeld-I to Bulk and Periodic Materials"'. *J. Comput. Chem.* **2013**, *34*, 422−427.
(64) Vanpoucke, D. E. P. *Hive*, version 2.1, 2011, http://users.ugent.be/~devpouck/.
(65) Becke, A. D. A Multicenter Numerical-Integration Scheme for Polyatomic-Molecules. *J. Chem. Phys.* **1988**, *88*, 2547−2553.
(66) Lebedev, V. I.; Laikov, D. N. Quadrature Formula for the Sphere of 131th Algebraic Order of Accuracy. *Dokl. Akad. Nauk* **1999**, *366*, 741−745.
(67) Momma, K.; Izumi, F. VESTA 3 for Three-Dimensional Visualization of Crystal, Volumetric and Morphology Data. *J. Appl. Crystallogr.* **2011**, *44*, 1272−1276.

(68) Smit, B.; Maesen, T. L. M. Molecular Simulations of Zeolites: Adsorption, Diffusion, and Shape Selectivity. *Chem. Rev.* **2008**, *108*, 4125−4184.
(69) Widom, B. Potential-Distribution Theory and the Statistical Mechanics of Fluids. *J. Phys. Chem.* **1982**, *86*, 869−872.
(70) Bae, Y.-S.; Snurr, R. Q. Development and Evaluation of Porous Materials for Carbon Dioxide Separation and Capture. *Angew. Chem., Int. Ed.* **2011**, *50*, 11586−11596.
(71) Potoff, J. J.; Siepmann, J. I. Vapor-Liquid Equilibria of Mixtures Containing Alkanes, Carbon Dioxide, and Nitrogen. *AIChE J.* **2001**, *47*, 1676−1682.
(72) Rappe, A. K.; Casewit, C. J.; Colwell, K. S.; Goddard, W. A.; Skiff, W. M. UFF, A Full Periodic-Table Force-Field for Molecular Mechanics and Molecular-Dynamics Simulations. *J. Am. Chem. Soc.* **1992**, *114*, 10024−10035.
(73) Mayo, S. L.; Olafson, B. D.; Goddard, W. A. DREIDING: A Generic Force-Field for Molecular Simulations. *J. Phys. Chem.* **1990**, *94*, 8897−8909.
(74) Dzubak, A. L.; Lin, L. C.; Kim, J.; Swisher, J. A.; Poloni, R.; Maximoff, S. N.; Smit, B.; Gagliardi, L. Ab Initio Carbon Capture in Open-Site Metal-Organic Frameworks. *Nat. Chem.* **2012**, *4*, 810−816.
(75) McDaniel, J. G.; Yu, K.; Schmidt, J. R. Ab Initio, Physically Motivated Force Fields for CO_2 Adsorption in Zeolitic Imidazolate Frameworks. *J. Phys. Chem. C* **2012**, *116*, 1892−1903.
(76) Verstraelen, T. *CMM Software*, 2013, http://molmod.ugent.be/software.
(77) Van Heest, T.; Teich-McGoldrick, S. L.; Greathouse, J. A.; Allendorf, M. D.; Sholl, D. S. Identification of Metal-Organic Framework Materials for Adsorption Separation of Rare Gases: Applicability of Ideal Adsorbed Solution Theory (IAST) and Effects of Inaccessible Framework Regions. *J. Phys. Chem. C* **2012**, *116*, 13183−13195.
(78) Hanson, R. M. Jmol − A Paradigm Shift in Crystallographic Visualization. *J. Appl. Crystallogr.* **2010**, *43*, 1250−1260.